Angular dependence of sampling modulation transfer function

O. Hadar, A. Dogariu, and G. D. Boreman

Sampling modulation transfer function (MTF) as defined in Park *et al*. [Appl. Opt. **23,** 2527–2582 (1984)] as an x and y sampling can be generalized for image data not along x and y directions. For a given sampling lattice (such as in a laser printer, a scene projector, or a focal-plane array), we construct a two-dimensional sampling MTF based on the distance between nearest samples in each direction. Because the intersample distance depends on direction, the sampling MTF will be best in the directions of highest spatial sampling and poorer in the directions of sparse sampling. We compare hexagonal and rectangular lattices in terms of their equivalent spatial frequency bandwidth. We filter images as a demonstration of the angular-dependent two-dimensional sampling MTF.

1. Introduction

We investigate the effect of two-dimensional (2-D) sampling on image quality with two different lattice structures. A finite-sized sampling lattice yields discrete image-sampling directions and a sample-to-sample distance that varies with direction. Angles with close nearest neighbors have high resolution while other angles produce poorer resolution. The number of angles and the distance between samples determine the image quality resulting from the sampling process. As we increase the number of lattice points, the number of possible discrete angles increases and the total resolution increases. In the first section the mathematical development for average sampling modulation transfer function (MTF) in one dimension is derived. Next we describe the derivation of a nonseparable 2-D sampling MTF from the definition of the one-dimensional (1-D) average sampling MTF. The process of obtaining the MTF is then demonstrated on two different lattices, rectangular and hexagonal. An equivalent bandwidth for the MTF is defined in the next section on the basis of noise-equivalent bandwidth. This figure of merit is used for comparison of different lattice sizes and configurations. We then present a simulation of these results on a test image.

2. Average Sampling Modulation Transfer Function

Previous work in sampling MTF[1–4] has been performed only in the context of x- and y-domain sampling. Here we consider not only the two orthogonal directions but also all other possible directions. Any sampling grid has different spatial sampling rates in different directions. We present the sampling MTF for a 2-D sampling system. This analysis has applications to laser-printer systems, infrared scene projectors, and focal-plane arrays.

In the case of sampling by 2-D array of finite-sized pixels, there are two distinct MTF contributions involved: one for the sampling process associated with the finite spacing between samples, and one for the spatial-averaging process associated with the finite size of the pixels. We assume that these two MTF's multiply to yield an aggregate MTF for the sampling-and-averaging process. The multiplication of MTF's is dependent on assumptions of linearity and shift invariance. The definition[1] of the sampling MTF in terms of an average over all possible positions of the scene with respect to the sampling locations essentially defines a shift-invariant sampling MTF. This separation of the MTF contributions allows our analysis of sampling MTF to proceed, considering only the locations of the samples (essentially assuming point receivers) and accounting for the finite pixel size by the pixel MTF.

O. Hadar is with the Department of Electrical and Computer Engineering, Ben-Gurion University of the Negev, P.O. Box 653, 84105 Beer-Sheva, Israel. A. Dogariu and G. D. Boreman are with the Department of Electrical Engineering, Center for Research and Education in Optics and Lasers, University of Central Florida, Orlando, Florida 32816-2700.

Received 3 February 1997; revised manuscript received 9 June 1997.

0003-6935/97/287210-07$10.00/0

The MTF contribution of finite-sized pixels is already well known. For a 1-D rectangular pixel, the pixel MTF is given by the sinc function formula,

$$\mathrm{MTF}_{\mathrm{pixel}} = \mathrm{sinc}(\xi p), \tag{1}$$

where $\mathrm{sinc}(x) = (\sin \pi x)/(\pi x)$, ξ is the image spatial frequency, and p is the pixel size. The square pixel is the most common shape for imaging-array applications although other shapes such as circular, hexagonal,[5] or tapered[6] are possible. As shown in Refs. 5 and 6, the pixel MTF is in general two dimensional.

In this research we consider the MTF of the 2-D angular dependence of the sampling process. The 2-D pixel MTF must also be included (multiplicatively) in the complete analysis, but because it is already well known, we do not develop it further and we present our development only for the sampling MTF.

The MTF in Eq. (1) does not account for the distance between the samples. We derive the sampling MTF from the pixel MTF [Eq. (1)]. The independence of these two processes allows us to multiply these two MTF's to derive the total MTF of the sampling and spatial-averaging process. In this research we concentrate on the sampling MTF.

The sampling MTF results from a reduction in measured modulation depth because the image data can exist at a random location with respect to the sampling sites. Park *et al.*[1] performs an average MTF calculation over all relative positions of the image data with respect to the sampling sites. This statistical approach performs an average of the shift-variant image quality that is seen in sampled data systems to define a shift-invariant average MTF. The derivation of the 1-D sampling MTF is based on a statistical treatment of the intensity sampled by the array of pixels.[1–3] The image-quality effect of sampling is equivalent to a convolution of the image data with a rectangular function, whose width is equal to the sampling interval.[1] Thus, the sampling MTF is a sinc function, with first zero equal to the inverse of the sampling interval.

The sinc function[1] can be obtained in a simple intuitive manner. Assume a sinusoid with a spatial period X and unity amplitude. We calculate the expected value of the modulation depth M of this sinusoid as a function of spatial sampling interval Δ and the spatial frequency $\xi = 1/X$. The sampling grid statistically can have any phase φ with respect to the maxima and the minima of the sinusoid.

We can begin with the expression for modulation depth,[3]

$$M(\xi, \Delta, \varphi) = (A_{\max} - A_{\min})/2, \tag{2}$$

where $A_{\max}$ and $A_{\min}$ are, respectively, the maximum and the minimum sampled values. If we define φ as the smallest distance between the sampling grid and the positive crest of the sine waves measured from this crest, φ varies between $\varphi_{\min} = -\Delta/2$ and $\varphi_{\max} = \Delta/2$. Two extreme cases for the value of M can be obtained from the sampling process. The maximum value is obtained for $\varphi = 0$, $M_{\max} = 1$ while the minimum value $M_{\min}$ is obtained for $\varphi = \varphi_{\min} = -\Delta/2$ or $\varphi = \varphi_{\max} = \Delta/2$. The value of $M_{\min}$ can be found with a simple trigonometric identity,

$$M_{\min} = 2 \cos\left(2\pi\xi \frac{\Delta}{2}\right)/2 = \cos(\pi\xi\Delta). \tag{3}$$

Between the extreme cases $\mathrm{MTF}_{\min}$ and $\mathrm{MTF}_{\max}$ are many different MTF's that can be derived from different values of the phase φ between the sine wave and the sampling grid. It is possible to obtain the average MTF by performing averaging over all possible locations of the sampling lattice with respect to the waveform. The assumption is that the random variable φ is equally distributed between $\varphi_{\min} = -\Delta/2$ and $\varphi_{\max} = \Delta/2$ with a uniform probability density function,

$$f_{\varphi}(\varphi) = \begin{cases} 1/\Delta & \text{for } -\Delta/2 \le \varphi \le \Delta/2 \\ 0 & \text{elsewhere} \end{cases}. \tag{4}$$

The average MTF (AMTF) is defined by the integral,

$$\begin{aligned} \mathrm{AMTF}_{\mathrm{samp}}(\xi, \Delta) &= \int_{-\Delta/2}^{\Delta/2} f_{\varphi}(\varphi) M(\xi, \Delta, \varphi) \mathrm{d}\varphi \\ &= \frac{1}{\Delta} \int_{-\Delta/2}^{\Delta/2} \cos(\pi\xi\varphi) \mathrm{d}\varphi = \mathrm{sinc}(\xi\Delta). \end{aligned} \tag{5}$$

The result of Eq. (5) can be interpreted as follows. For a nonzero sampling interval of Δ, we do not obtain the true maxima and minima of the sinusoid on an average basis but instead obtain an average maximum value and an average minimum value of the sinusoid that are the average values of the waveform over the interval Δ. The maximum average value of the waveform is the average of the peak of the sinusoid over an interval Δ, while the minimum average value of the waveform is the average of the valley of the sinusoid over the same interval. This conceptual model yields the main result of Park *et al.*,[1] namely the sinc function with the first zero location $\xi_{\mathrm{cutoff}} = 1/\Delta$. Even for very sparse sampling, where the spatial sampling interval Δ is less than the Nyquist requirement of $1/2X$, the notion of an average maximum value and an average minimum value is still valid, even when the averaging is performed over an interval Δ that is greater than half the period of the waveform.

We can modify the result of Eq. (5) for the case of 2-D sampling by representing the MTF for the two orthogonal axes x and y,

$$\mathrm{MTF}(\xi) = \mathrm{sinc}(\xi\Delta_x) = \frac{\sin(\pi \cdot \xi \cdot \Delta_x)}{(\pi \cdot \xi \cdot \Delta_x)}, \tag{6a}$$

$$\mathrm{MTF}(\eta) = \mathrm{sinc}(\eta\Delta_y) = \frac{\sin(\pi \cdot \eta \cdot \Delta_y)}{(\pi \cdot \eta \cdot \Delta_y)}, \tag{6b}$$

where ξ and η are the spatial frequencies in the x and y axes, respectively, and Δ_x and Δ_y are the sampling

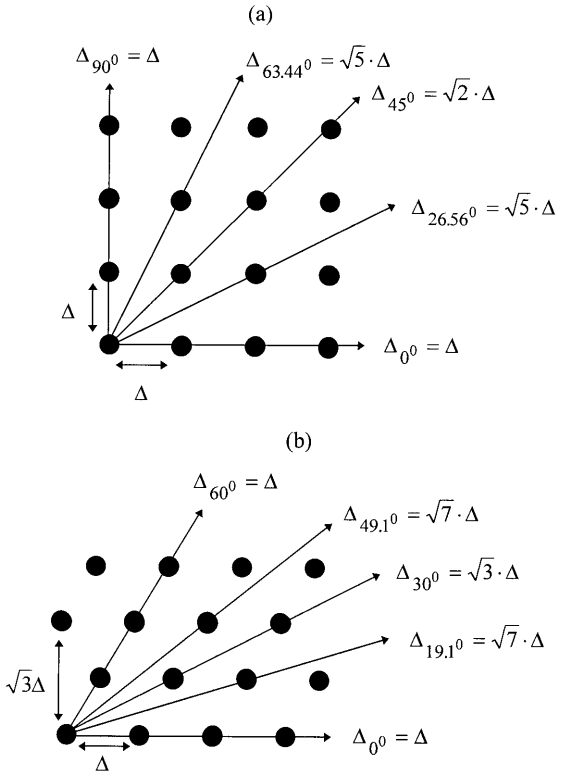

Fig. 1. 4×4 lattice size with the high-resolution directions marked by arrows: (a) rectangular lattice, (b) hexagonal lattice.

interval in the x and y axes, respectively. We allow the MTF to be a bipolar function rather than use the magnitude.

Note that these equations do not imply a separable 2-D MTF as the product of Eqs. (6a) and (6b). The sampling interval and associated sampling MTF for spatial frequencies not along x or y will be calculated separately.

3. Definition of Nonseparable Two-Dimensional Sampling Modulation Transfer Function

In this section the main steps of deriving the sampling MTF for both rectangular and hexagonal lattices are described. We develop the MTF not only along ξ and η but also along the other directions that are involved in the sampling process. For any given lattice, there are directions with relatively smaller sampling intervals. Image information in those directions is reproduced with higher fidelity than image information in those directions for which sampling is less frequent. These directions can be derived from all the possible lines that can be reproduced by the lattice. We assume that each of these lines passes through the exact center of sampling points in the grid. Our research extends the research of previous authors mainly in that we use the sinc function of Eq. (5) as valid for any sampling direction in a 2-D lattice. This allows us to calculate a sampling MTF in any direction of the lattice.

We show portions of the two sampling lattices (rectangular and hexagonal) investigated in Figs. 1(a) and 1(b). We define the distance between two adjacent points of the rectangular lattice in the x and y directions as Δ. If we take the lower left point of the grid as the origin of the lattice, any other point in the lattice has a certain distance from the origin, Δ_θ, which is a function of Δ and θ, the angle between the point and the positive direction of the x axis. For example, the sampling distances for the five highest-resolution directions in the lattice in a sector of 90° are $\Delta_{0^\circ} = \Delta_{90^\circ} = \Delta$, $\Delta_{45^\circ} = \sqrt{2} \cdot \Delta$, and $\Delta_{26.56^\circ} = \Delta_{63.44^\circ} = \sqrt{5} \cdot \Delta$. For other angles the sampling is less frequent, and the sinc function associated with the sample-to-sample distance will have a correspondingly lower cutoff frequency. The sinc function MTF of Eq. (5) can be generalized to a nonseparable equation in terms of a 2-D spatial frequency ξ_θ, where the wave vector for any particular spatial frequency is along the θ direction,

$$\mathrm{MTF}(\xi_\theta) = \mathrm{sinc}(\xi_\theta \Delta_\theta) = \sin(\pi \xi_\theta \Delta_\theta)/(\pi \xi_\theta \Delta_\theta). \quad (7)$$

In Fig. 1(b) the same analysis is implemented for the hexagonal lattice. Let us set the sampling distance along the x direction, $\Delta_{0^\circ} = \Delta$, to be equal for both the square lattice and the hexagonal lattice. We construct the hexagonal lattice from the rectangular lattice by moving the odd rows a distance of $\Delta/2$ to the right and setting the distance between rows in the vertical direction to $(\sqrt{3}/2)\Delta$. This configuration provides us a symmetric lattice within a 60° sector. This kind of lattice is particularly appropriate for printing applications because it is the most compact lattice[7] for round pixels.

For the hexagonal lattice of Fig. 1(b), the minimum sample distance is $\Delta_{0^\circ} = \Delta_{60^\circ}$. The highest-resolution directions in the 60° sector with their sampling distances are $\Delta_{0^\circ} = \Delta_{60^\circ} = \Delta$, $\Delta_{30^\circ} = \sqrt{3} \cdot \Delta$, and $\Delta_{19.1^\circ} = \Delta_{49.1^\circ} = \sqrt{7} \cdot \Delta$. The MTF here is also a function of the sampling direction as in Eq. (7). The application of Eq. (7) will yield a nonseparable MTF with sinc functions in each direction. This function is difficult to visualize because of its discontinuous variation with angle.

Figures 2(a) and 2(b) represent the three highest-resolution MTF's in the rectangular lattice and the hexagonal lattice, respectively, plotted as functions of $|\xi_0|$.

We can obtain a more complete picture of the angular dependence of the MTF by using a top view. In Fig. 3 we plot a line in each direction; the length of the line in that direction is equal to the distance along ξ_θ to the first zero of the sinc function in that direction. Figures 3(a) and 3(b) show the results in a 90° sector for a 10×10 lattice size for both rectangular lattice and hexagonal lattice, respectively. A long line in a certain direction represents high resolution in that direction. For each lattice, the MTF is a discontinuous function of angle θ, with some directions having high resolution, some having low resolution, and some directions having MTF = 0 (no sampling in that direction for a finite-sized lattice).

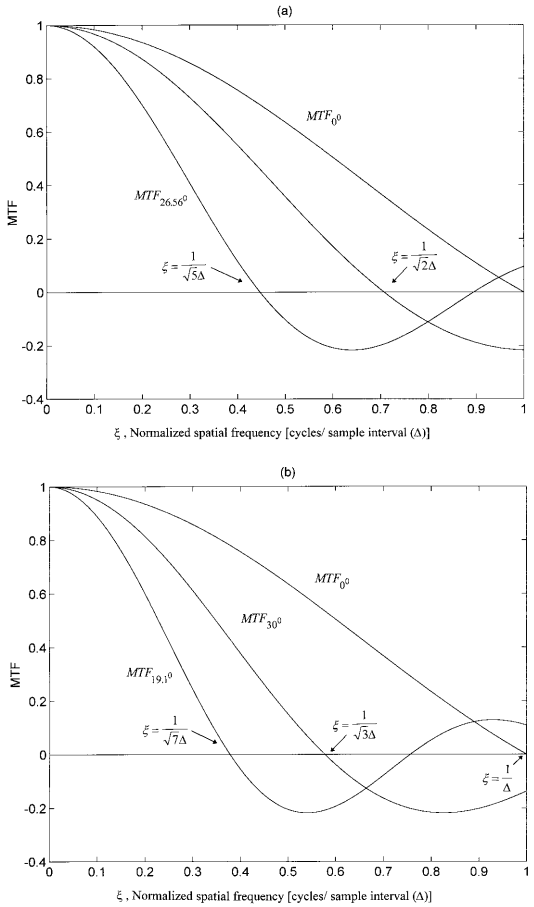

Fig. 2. Three highest-resolution MTF's in a 1-D plot: (a) rectangular lattice, (b) hexagonal lattice.

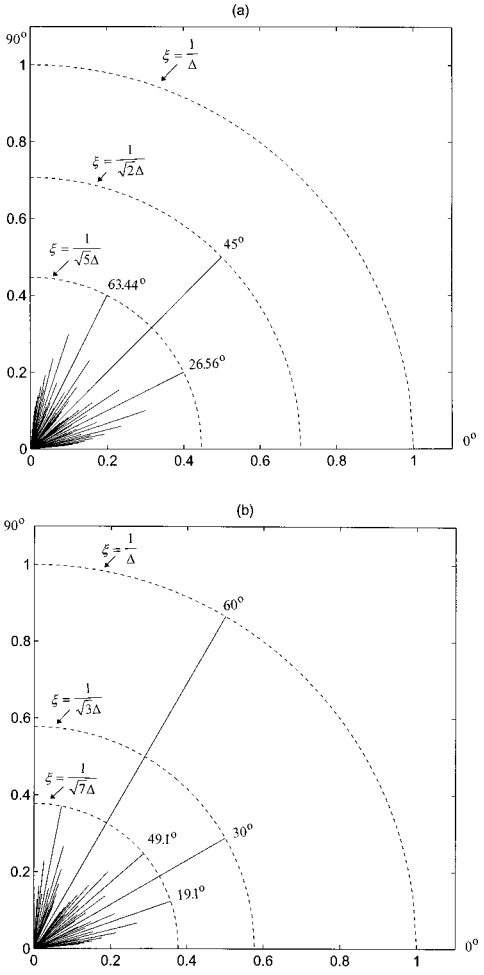

Fig. 3. First zero location of the MTF as function of the angle θ in a radial plot: (a) rectangular lattice, (b) hexagonal lattice.

4. An Equivalent-Bandwidth Figure of Merit

In this section we define a useful measure for quantifying the sampling process. The equivalent bandwidth of the sinc function for any direction in the lattice is derived. A common definition for equivalent bandwidth is the equivalent-noise bandwidth.[8] We thus define an angle-dependent bandwidth:

$$\mathrm{BW}_\theta = \frac{1}{\mathrm{MTF}_\theta(0)} \int_0^\infty \mathrm{MTF}_\theta(\xi)\mathrm{d}\xi, \tag{8}$$

where $\mathrm{MTF}_\theta(\xi)$ is the MTF in a certain angle θ relative to the x direction, and $\mathrm{MTF}_\theta(0)$ is the maximum value of the MTF, which is unity. To compare the image-quality performance for various lattice sizes and configurations, we use the equivalent bandwidth (BW) of the sinc function as the MTF in Eq. (8),

$$\mathrm{BW}_\theta = \int_0^\infty \mathrm{sinc}(\xi_\theta \Delta_\theta)\mathrm{d}\xi = \frac{1}{\Delta_\theta}. \tag{9}$$

Equation (9) has the simple geometric interpretation as the distance to first zero ($1/\Delta_\theta$), which defines the ξ_{cutoff} of the sinc function, shown as the length of the line in the plot in Fig. 3.

We can write BW_θ in each possible direction of the lattice as function of Δ, which is the basic sampling interval along the x axis ($\Delta_{0^\circ} = \Delta$),

$$\mathrm{BW}_\theta = \frac{1}{\Delta_\theta} = k_\theta \frac{1}{\Delta}, \tag{10}$$

where k_θ is a constant that represents the length of a certain line in Fig. 3 in units of $1/\Delta$. To construct a figure of merit for any given lattice, we sum up the BW's for all the possible directions. This gives a total BW, $\mathrm{BW}_{\mathrm{total}}$, for the sampling lattice and can be interpreted as the area in polar coordinates under the curves plotted in Fig. 3,

$$\mathrm{BW}_{\mathrm{total}} = \sum_{\theta=0^\circ}^{\theta=90^\circ} \mathrm{BW}_\theta = \sum_{\theta=0^\circ}^{\theta=90^\circ} k_\theta \frac{1}{\Delta} = K \frac{1}{\Delta}, \tag{11}$$

where K is the sum of all the k_θ constants that exist between $\theta = 0°$ and $\theta = 90°$.

The new measure $\mathrm{BW}_{\mathrm{total}}$ allows us to investigate the influence on the image quality of an increase in the lattice size. The difference in image quality when a larger lattice is used is twofold: one increase is from the larger number of angles for which there exists a nearest neighbor. This tends to fill in the

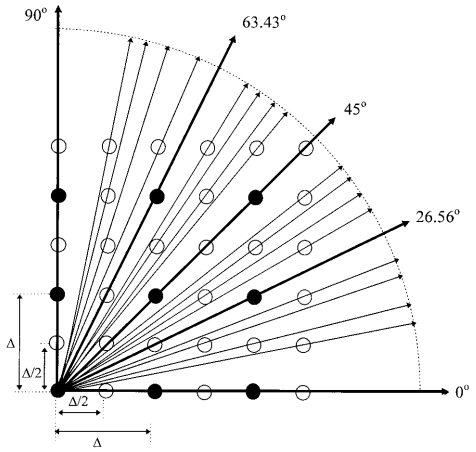

Fig. 4. Scaling the cutoff frequency by doubling the lattice size, original 3 × 3 points rectangular lattice (closed circles), 6 × 6 points rectangular lattice (open circles).

angles for which the MTF is small but not exactly equal to zero. The second and more important reason for an increase in image quality when a larger lattice is used is that for a given image field size, more sampling points imply a higher spatial sampling rate with higher cutoff frequencies in all directions.

In Fig. 4 the influence of a doubling of the lattice size on the total frequency bandwidth of the sampling system is demonstrated. The original rectangular lattice has a size of 3 × 3 points (closed circles) with sampling interval of Δ in the two main orthogonal axis directions x and y. There are five angles for this case, and they are marked by the thick arrows at 0°, 26.56°, 45°, 63.43°, and 90°. The higher-resolution lattice shown as the 6 × 6 array of open circles contains twice the number of points as the lower-resolution lattice. The sampling rate increases by factor of 2 in these directions, and the sampling interval decreases from Δ to Δ/2 in the x and y directions.

The second reason for increasing the resolution is the additional angles in the higher-resolution lattice. More than 20 possible directions (thin short arrows) are seen as four new directions between each two of the former directions. These angles contribute to the summation of BW_θ in the larger lattice.

For comparison of different lattice configurations on this basis (square versus hexagonal), we keep the total number of lattice points equal (100 points in a 10 × 10 square and 100 points in the hexagonal). This allows us to compare directly the $\mathrm{BW}_{\mathrm{total}}$ as a figure of merit. The results for this comparison are for the rectangular lattice $\mathrm{BW}_{\mathrm{total}} = 111.44\ [Cy/\Delta]$ and for the hexagonal lattice $\mathrm{BW}_{\mathrm{total}} = 126.01\ [Cy/\Delta]$. There is a benefit of 13% from the use of the hexagonal lattice compared with the use of the rectangular lattice for a 10 × 10 lattice size.

We investigate the influence of an increase in the number of points of the lattice in 1-D N (lattice size equal to $N \times N$) on the total number of angles. Figure 5 represents the number of angles possible for

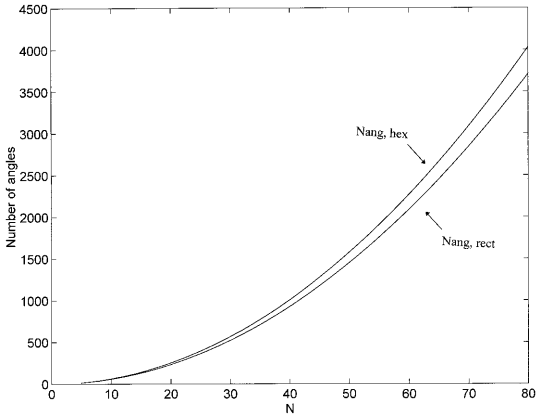

Fig. 5. Number of possible angles as a function of number of points in 1-D, N (lattice size equals $N \times N$ points).

both the rectangular and the hexagonal lattices as a function of N. We take the lower left point of the grid and consider it as the reference point for the all other points in the lattice.

For both lattices, increasing the number of points of the lattice produces more possible angles. However the rate of increase of possible angles in the case of the hexagonal lattice is higher than in the case of the rectangular lattice. Analytical functions are fitted for both the numerical functions in Fig. 5, yielding $0.58N^2$ for the rectangular lattice and $0.63N^2$ for the hexagonal lattice. Hence there are 8.6% more angles in the hexagonal lattice than in the rectangular lattice for the same number of sampling points in the lattice.

5. Influence of N on $\mathrm{BW}_{\mathrm{total}}$

We now discuss the influence of an increase in the number N on the new measure $\mathrm{BW}_{\mathrm{total}}$. The basis for this calculation is the maintenance of the lattice size at a constant value and the change of only the number of points in the lattice. By incrementing the number of lattice points, we decrease the sampling distance and scale the spatial frequency each time to the new sampling rate. Figure 6 represents the results for $\mathrm{BW}_{\mathrm{total}}$ for both the rectangular and the

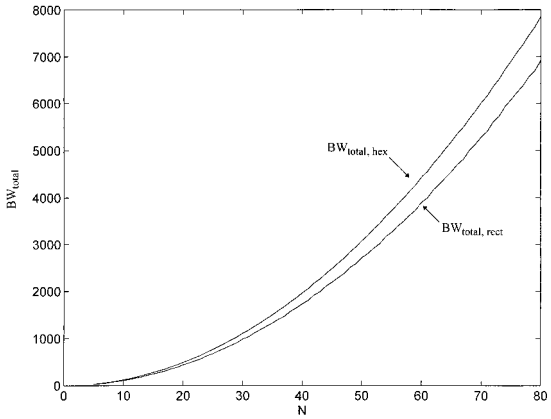

Fig. 6. Total equivalent bandwidth $\mathrm{BW}_{\mathrm{total}}$ as function of N.

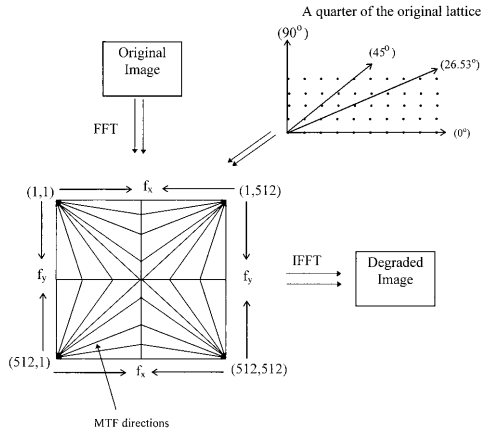

Fig. 7. Description of the degradation process.

hexagonal lattice, where BW_{total} is plotted as function of N. As we expected, BW_{total} increases with an increase in the value of N for both lattices because both the sampling rate and the number of possible angles increase. BW_{total} is always higher for the hexagonal lattice. This result was expected because the distance between rows in the hexagonal lattice is smaller by 15.4% when compared with the rectangular lattice, and the number of angles in the hexagonal lattice is higher. Analytical functions for the dependence of BW_{total} of N were fitted to the numerical results. For the rectangular lattice BW_{total} was $1.09N^2$, and for the hexagonal lattice BW_{total} was $1.23N^2$. The benefit of choosing the hexagonal lattice for any lattice size is 13%.

6. Pictorial Comparison–Demonstration

We constructed the sampling MTF for a given lattice size and configuration. The original image is 512 × 512 pixels. The degradation process is described by the block diagram in Fig. 7. The first step is to derive all the possible directions for which information can be reproduced by the lattice in a sector of 90° (a quarter of the original sampling lattice size). For our purposes the origin of the lattice is the center point of the lattice. The next step is to associate a sinc function with each of these directions and scale the cutoff of the sinc to correspond with the desired cutoff frequency. The MTF is then multiplied by the Fourier transform of the original image. The sampling degradation is associated only with a decrease of the amplitude. The MTF is thus applied only on the magnitude of the image Fourier transform. Therefore, the original phase is kept while the amplitude is degraded by the MTF. The lines in Fig. 7 indicate the existing directions for a given lattice, for which the amplitude is multiplied by the MTF. In all the other directions the image amplitude is set to zero. Using the degraded amplitude function com-

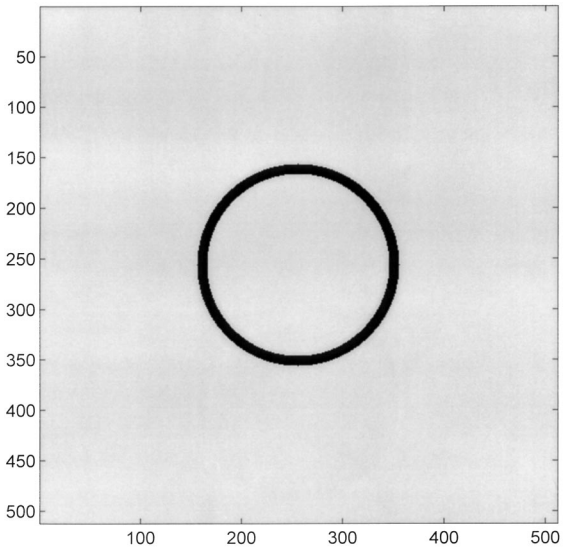

Fig. 8. Original image.

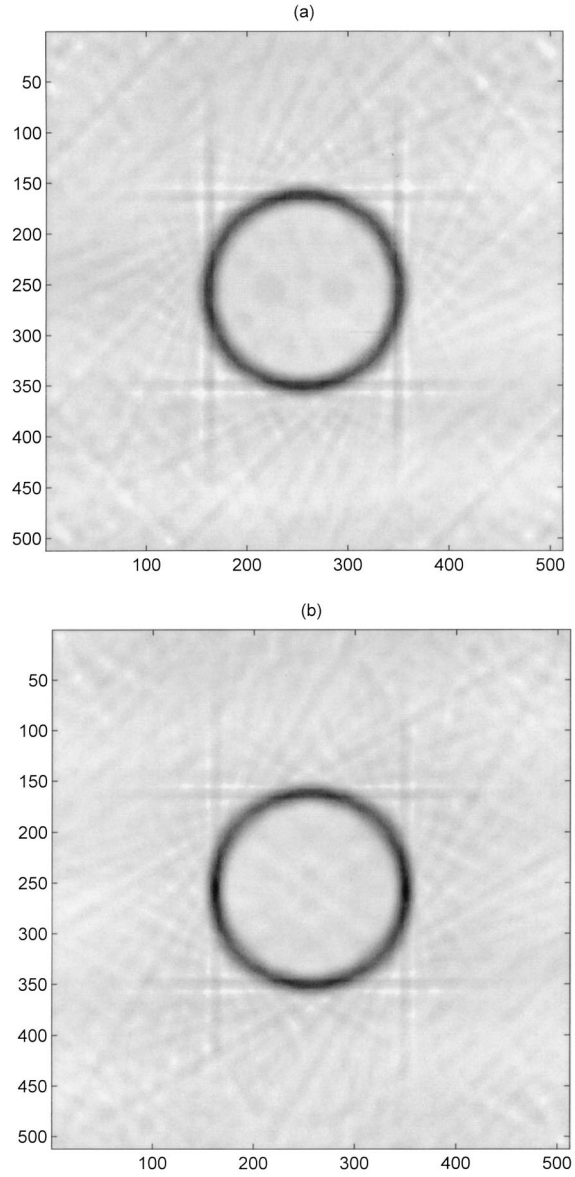

Fig. 9. Degraded image by a sampling MTF of 100 × 100 points lattice size: (a) rectangular lattice, (b) hexagonal lattice.

bined with the original phase function and taking the inverse Fourier transform, we obtain the degraded image in the spatial domain.

The original image is plotted in Fig. 8; it is a black ring on a white background, with a width of 10 pixels and an inner radius of 90 pixels. The image is degraded by a sampling MTF that corresponds to a 100×100 lattice size. Results for the rectangular lattice and the hexagonal lattice are presented in Figs. 9(a) and 9(b), respectively. The degraded image is affected differently for different angles. The blur size is not equal in all the directions of the blurred image. In the image degraded by the rectangular lattice [Fig. 9(a)] the least degraded directions are the x and y directions. This phenomenon can be shown by the sharp edges of the thin lines in these directions. All the other directions are more degraded and have smeared edges. Also it can be shown that the degraded image is symmetrically degraded within one cycle of the 90° sector.

In the image degraded by the hexagonal lattice [Fig. 9(b)] it can be seen that the two lines perpendicular to the x direction are sharper than the lines that are perpendicular to the y direction. The reason is that in the hexagonal lattice the resolution in the x direction is higher than the resolution in the y direction by a factor of $\sqrt{3}$.

7. Conclusions

An average MTF for the sampling process is obtained by an average over the sampling locations. The resulting MTF is the sinc function with the first zero location at the reciprocal of the sampling interval. The sinc function MTF is generalized to a nonseparable MTF in terms of a 2-D spatial frequency at all the possible directions of the sampling lattice. We extend this research beyond that of previous authors in that we use the sinc function as valid for any sampling direction in a 2-D lattice. The MTF derivation is demonstrated for two lattice configurations, the rectangular lattice and the hexagonal lattice. A useful quantitative measure is defined as the total equivalent bandwidth of the sampling lattice; this measure allows us to compare different lattice configurations and sizes. A pictorial demonstration is presented for two different lattices.

This study was supported by the Hewlett-Packard University Grants Program and the Clore Scholar Foundation for doctoral students in Israel.

References

1. S. K. Park, R. Schowengerdt, and M. A. Kaczynski, "Modulation-transfer-function analysis for sampled image systems," Appl. Opt. **23,** 2572–2582 (1984).
2. K. M. Hock, "Effect of oversampling in pixel arrays," Opt. Eng. **34,** 1281–1288 (1995).
3. L. de Luca and G. Cardone, "Modulation transfer function cascade model for a sampled IR imaging system," Appl. Opt. **13,** 1659–1664 (1991).
4. W. Wittenstein, J. Fontanella, A. Newberry, and J. Baars, "The definition of the OTF and the measurement of aliasing for sampled-imaging systems," Opt. Acta **29,** 41–50 (1982).
5. K. J. Barnard and G. D. Boreman, "Modulation transfer function of hexagonal staring focal plane arrays," Opt. Eng. **30,** 1915–1919 (1991).
6. G. Boreman and A. Plogstedt, "Spatial filtering by a line-scanned nonrectangular detector: application to SPRITE readout MTF," Appl. Opt. **28,** 1165–1168 (1989).
7. N. W. Ashcroft and N. D. Mermin, *Solid State Physics* (Saunders College, Philadelphia, Pa., 1976), pp. 63–83.
8. R. D. Hudson Jr., *Infrared System Engineering* (Wiley, New York, 1969), pp. 311–315.